The Influence of Rubber Inclusion on the Dynamic Response of Rail Track

Yujie Qi, Ph.D., A.M.ASCE[1]; Buddhima Indraratna, Ph.D., F.ASCE[2];

[1]Lecturer, and Program Co-leader of Transport Research Centre, School of Civil and Environmental Engineering, University of Technology Sydney, Sydney NSW 2007, Australia. Email: yujie.qi@uts.edu.au

[2]Distinguished Professor of Civil Engineering, Founding Director of Australian Research Council's Industrial Transformation Training Centre for Advanced Technologies in Rail Track Infrastructure (ITTC-Rail), Director of Transport Research Centre, School of Civil and Environmental Engineering, University of Technology Sydney, Sydney, NSW 2007, Australia. Email: buddhima.indraratna@uts.edu.au

†Author for correspondence:
Yujie Qi
Lecturer & Program Co-leader of Transport Research Centre,
Faculty of Engineering and Information Technology,
University of Technology Sydney,
Email: Yujie.qi@uts.edu.au

ABSTRACT: Heavier and faster trains have motivated researchers to seek better ways to absorb the increasing amount of energy imparted to rail foundations and mitigate track deterioration. In recent years resilient rubber products have attracted more attention due to the high level of damping and the associated energy absorbing capacity of rubber. However, since rubber granules have lower shear strength and higher compressibility compared to natural rock aggregates, a better understanding of how rubber inclusions can influence the track system is imperative, especially before putting these recycled resilient materials into practice. In this paper, the performance of rail track incorporating an alternative subballast layer, i.e. a synthetic energy absorbing layer (SEAL) consisting of a mixture of granulated rubber and mining waste is evaluated through large-scale prismoidal triaxial tests and a computational dynamic model. It is revealed that the amount of granulated rubber in SEAL composites has a significant influence on the dynamic behaviour of the track. Fundamentally, increasing the amount of rubber within SEAL leads to a higher vertical deformation, increased energy absorbing capacity, and a higher damping ratio and vibration level, while reducing the ballast degradation, track stiffness and lateral movement (dilation) of the track. It has been found that 10% of rubber by mass is the optimal amount of rubber to be included in SEAL. This amount of rubber will ensure that a ballasted track can efficiently reduce the dynamic contact pressure at the interface between different track layers (i.e. sleeper, ballast, subballast, and subgrade), as well as reduce the lateral spread (dilation) and breakage of ballast without generating excess vibration and settlement comparing to traditional track materials.

Keywords: recycled rubber; dynamic loading; ballast degradation; railway foundation; large-scale laboratory tests; track dynamic model.

1. Introduction

Due to the increasing demand for passenger and freight transportation, railways are now operating heavier and faster trains. As a result, the dynamic loads from moving stock lead to higher stresses and exacerbated ground vibration for track substructure, which in return damage the track components, escalate track deterioration (e.g. ballast degradation and track displacement), and increase the risk of derailment. Consequently, more frequent track maintenance is required, which then increases the cost of maintenance. Various techniques have been proposed to mitigate these adverse effects such as improving track foundations by including resilient components and geosynthetics, and attenuating ground vibrations from the source or receiver (Fernandes et al. 2008, Indraratna and Nimbalkar 2013, Tatsuoka et al. 2014, Toward et al. 2014, Fathali et al. 2019). Of these techniques, researchers and practitioners are realising that the inclusion of rubber materials such as recycled tyre cells, under-ballast shock mats, under-sleeper pads, and granulated rubber added to the compacted capping layer or to the ballast later itself can be beneficial options; this is because their higher damping properties and greater energy absorbing capacity help the track system to dissipate the energy from the dynamic (moving) loading and thereby mitigate the damage to rail tracks (Indraratna et al. 2020, Qi and Indraratna 2020).

Previous studies found that installing rubber shock-mats beneath the sleepers or ballast stratum can significantly reduce ballast degradation and the stresses developed at the ballast-sleeper interface, while increasing the damping ratio and energy absorption capacity of the track system (Lakušić et al. 2010, Nimbalkar et al. 2012, Sol-Sánchez et al. 2014, Kaewunruen et al. 2017, Navaratnarajah and Indraratna 2017, Indraratna et al. 2018a, Indraratna et al. 2019, Jayasuriya et al. 2019, Ngo et al. 2019). Xin and Gao (2011) found that installing rubber mats in tracks over a concrete bridge deck reduces the vertical acceleration of the rail by almost 73% as the train passes over at high speed (over 250 km/h). Indraratna et al. (2018c) used recycled tyre cells to confine crushed basalt forming the capping layer. Large-scale testing and numerical modelling have shown a reduction in lateral and vertical deformation, as well as lower ballast degradation and higher bearing capacity. Apart from rubber mats/pads and recycled tyre cells, granulated rubber or rubber crumbs have also proven to be alternative options for use in rail tracks. Tyre-derived aggregates mixed with ballast have been proposed by other researchers (Sol-Sánchez et al. 2015, Esmaeili et al. 2017, Gong et al. 2019) to reduce particle breakage and abrasion during tamping and subsequent track operations. Indraratna et al. (2018b) developed a synthetic energy absorbing layer (SEAL) by mixing rubber crumbs with industry by-products (e.g. steel furnace slag and coal wash) used as a subballast layer. The authors have carried out small-scale and large-scale laboratory tests to examine the performance of the SEAL mixture and found that with a proper amount of rubber the SEAL can reduce ballast degradation and maintain acceptable stiffness and deformation (Qi et al. 2018b, Qi and Indraratna 2020). Since all these rubber inclusions can be manufactured from waste tyres, the resulting improvements are carbon-friendly and economically attractive.

Despite the obvious advantages of using rubber materials, there are still some concerns about including these soft materials in track foundations. In general, the more resilient a track is, the smaller the dynamic wheel load generated from impact will be, which suggests that since the track modulus represents the overall stiffness of the rail foundation, it should not be overly high. However, a relatively low track modulus indicates a softer rail foundation which may lead to ballast or subgrade problems such as extensive deformation and vibration or even "bounciness" (Li and Selig 1995). In fact, when more rubber products are included, the track specimens present a lower track modulus with increasing deformation as reported (i) for a tyre cell reinforced capping layer (Indraratna et al. 2017), (ii) for granulated rubber mixed with ballast (Sol-Sánchez et al. 2015, Esmaeili et al. 2017), and (iii) for rubber-waste aggregate mixtures used as subballast (Qi et al. 2018a). Some soft ballast mats/under sleeper pads can suppress vibration in a relatively high frequency (i.e. 50 ~150 Hz), but not when the vibration is at a lower frequency (e.g. less than 30 Hz) (Kaewunruen and Remennikov 2016). Fernández et al. (2018) found that mixing 2.5-5% of granulated rubber with ballast reduced peak acceleration in the ballast layer by 20-55%, but the other layers experienced increased vibration. This is why investigating what mechanisms and how much rubber inclusions are needed to optimise the dynamic performance of the track before any further field applications is imperative, especially if the mixtures are to incorporate granulated rubber or rubber crumbs.

This paper focuses on the application of granulated rubber/rubber crumbs in rail tracks. It is a continuation of previous studies by the authors on the synthetic energy absorbing layer (SEAL) as a replacement for traditional subballast materials. Previous studies investigated the small scale static and cyclic loading behaviour of the SEAL matrix with different amounts of rubber, and they recommended that 10% of rubber can ensure an acceptable shear strength while enhancing the damping or energy absorbing properties (Indraratna et al. 2018b, Qi et al. 2019b, Indraratna et al. 2020). Qi and Indraratna (2020) also proposed an energy-based analysis which indicated that 10-13% rubber will dissipate the accumulated energy through an acceptable deformation in the SEAL layer and reduce ballast breakage. However, how the amount of rubber in a SEAL matrix can influence the dynamic performance of track (e.g. track modulus, damping property, vibration and dynamic loads at the interfaces between each layer) has not yet been addressed. Therefore, in this paper, the influence of the amount of rubber in SEAL on the dynamic response of track is investigated based on a series of large-scale laboratory testing in comparison with traditional track specimens. The displacement and acceleration of rail influenced by the amount of rubber within a SEAL matrix are also examined utilizing using a track dynamic model.

2. Large scale physical model for SEAL

2.1 Materials and test program

A large-scale physical model of the track was used to carry out a series of prismoidal triaxial tests to investigate the behaviour of the track that incorporates the SEAL matrix. This physical model has a ballast layer on top, a subballast layer in the middle and structural fill at the bottom, which simulates field conditions. The subballast layer was compacted with traditional subballast materials or the SEAL matrix containing varying amounts of rubber. These materials came from local suppliers, i.e., Bombo Quarry (NSW, Australia) for ballast, conventional subballast and structural rockfill, Australian Steel Milling Services for steel furnace slag (SFS), Illawarra Coal for coal wash (CW), and Tyre Crumbs Australia for rubber crumbs (RC). The grading curves of these materials are shown in Fig. 1.

The SEAL matrix was prepared by firstly mixing steel furnace slag with coal wash at a blending ratio of 7:3 by mass to ensure the mixture had sufficient strength while preventing the unacceptable swell pressure indicated by Indraratna et al. (2018b) and Qi et al. (2019b). Different rubber contents ($R_b = 0, 10, 20, 30$ and 40%) were added to the mixture and blended thoroughly to form the following SEAL matrices, i.e., SEAL0, SEAL10, SEAL20, SEAL30 and SEAL40, where the number immediately following the word 'SEAL' denotes the rubber content by weight. The rubber content is limited to 40% because a mixture with $R_b > 40\%$ will have a skeleton dominated by rubber, which is not applicable for civil engineering (Youwai and Bergado 2003). The grading curves for SEAL mixtures with different amounts of rubber are shown in Fig. 1.

The large-scale prismoidal triaxial facility (Fig. 2a) was used to examine the performance of the physical track model that incorporates SEAL. The testing chamber has a plan area of $600\ mm \times 800\ mm$ and a depth of 600 mm. Structural fill to a depth of 100 mm was compacted to the field dry density $\gamma_d of\ 21.4\ kN/m^3$at the bottom of the test chamber. The subballast layer (either traditional material or a SEAL matrix with different amounts of rubber) on top of the structural fill was compacted to a depth of 150 mm with the dry density achieving 95% of the maximum dry density. The maximum dry density $\gamma_{d,max}$ of traditional subballast material is $18.5\ kN/m^3$ with the optimum moisture content (OMC) of 4.5%; $\gamma_{d,max}$ of SEAL mixtures varies from 20.3 to 12.4 kN/m^3 as the rubber content increases from 0 to 40%, and OMC of SEAL mixtures remains within the range of 8-11%. A 200 mm thick layer of ballast with a bulk density of 15.3 kN/m^3 was then prepared on top of the subballast layer. A rail-concrete sleeper assembly with stiff E-type clip fastener system was placed on top of the ballast and then it was filled and levelled with shoulder ballast. A pressure cell was installed on top of each layer to detect the dynamic load (Fig. 2b). The ballast directly beneath the sleeper was painted for visual examination of breakage and collected after each test to determine the ballast breakage index (BBI).

The cyclic loading was applied with a loading frequency of 15 Hz and the maximum vertical stress under the sleeper was $q_{max} = 230\ kPa$ (Fig. 2c). This was to simulate the typical field conditions for an Australian freight train having a 25-tonne axle load running at a maximum speed of 110 km/h (Indraratna et al. 2018c, Navaratnarajah et al. 2018). Before each test, a conditioning phase with a loading frequency of 5 Hz over 100 cycles was applied to increase the contact area between the sleeper and the underlying ballast. During testing, the two sidewalls in the test chamber that are parallel to the sleeper were kept still, while the other two sidewalls (i.e. perpendicular to the sleeper) were allowed to move laterally under the confining pressure of 15 kPa. This was in order to simulate the condition of plane strain where deformation in the longitudinal direction of the track could be ignored. Each test was continued until $N = 500{,}000$ cycles, and there were six tests in total during which the subballast layer was composed of either traditional subballast or with the SEAL matrix ($R_b = 0, 10, 20, 30$ or 40%).

2.2 Deformation behaviour

The vertical displacement of the track specimen with the SEAL matrix and traditional subballast materials under cyclic loading is shown in Fig. 3a. As the amount of rubber (R_b) increases in the SEAL matrix the vertical displacement of the test specimen increases because of the increasing compressibility of the SEAL matrix as more rubber is added (Qi et al. 2018b). The vertical deformation of the test specimen increases rapidly in the first few thousands of cycles and then gradually stabilises as the accumulation rate of the vertical strain (ε_1) decreases with the increasing number of loading cycles (Fig. 3b). Here, the accumulation rate of ε_1 denotes the tangential slope of the total vertical strain versus loading cycles plot for two adjacent concerned points. Fig. 3b shows that there is a sharp reduction in the accumulation rate of vertical strain after it reaches 10^{-8}, which indicates that the increase in vertical deformation is negligible; in this case, the test specimen has apparently attained a state of 'plastic shakedown', which refers to a phenomenon where the granular aggregates under cyclic loading achieve a compacted assembly showing negligible vertical strain increment upon further loading (Lackenby et al. 2007). Except for SEAL40, the vertical deformation of all the test specimens attains plastic shakedown, albeit the specimen with traditional materials and SEAL0 reach plastic shakedown at around N=100,000 whereas others attain this condition at a later stage (N=300,000-400,000). Also note that the specimen with SEAL40 begins with a high accumulation rate of vertical strain (>10^{-4}, Fig. 4b-3) and fails at around N=1500 showing substantial settlement (> 40 mm) and pronounced vibration, which could be taken as plastic collapse.

Lateral displacement and the accumulation rate of lateral strain of all the test specimens are shown in Fig. 4. As expected, the lateral dilation of the track specimens decreases as more rubber is added to the SEAL matrix, but only for values of $R_b < 20\%$ (Fig. 4a). Except for the specimen with SEAL40, around 70% of the lateral dilation of other test specimens accumulates in the first 10,000 cycles (Fig. 4a) where the accumulation rate of the lateral strain begins at a magnitude of 10^{-6} and then gradually drops to a negligible level of 10^{-8} (Figs. 4b-1&2). It is noteworthy that when $R_b \geq 20\%$ the lateral displacement of the test specimen fluctuates with increasing loading cycles (Fig. 4a) as the accumulation rate alternates between negative and positive values (Fig. 4b-2). This occurs because when $R_b \geq 20\%$ the skeleton of the SEAL mixture is increasingly dominated by rubber, so the specimen tends to behave as rubber-like (Qi et al. 2018a, Qi et al. 2018c). For the test specimen with SEAL40, the accumulation rate of lateral stain is much higher at 10^{-3} than those specimens with smaller amounts of rubber (Fig. 4b-3); this means that lateral dilation has accumulated at a faster rate. Moreover, the changing sign of the accumulation rate for the specimen with $R_b \geq 20\%$ indicates an unstable lateral behaviour because lateral compression and dilation appear alternately (Fig. 4b-3).

The elastic vertical deformation of the test specimen shown in Fig. 5a is a good indicator of vertical vibration under cyclic loading (Qi and Indraratna 2020). It is noted that the elastic vertical deformation increases with the loading cycle and stabilises rapidly after 500 cycles. As the R_b in the SEAL matrix increases, the elastic vertical deformation of the track specimen increases. The elastic vetical deformation reflects the way of rubber-soil mixtures to release the energy via increased bounciness (up and down movement), hence inducing more vibration in the test specimen. In fact, the vertical displacement almost doubles when R_b increases from 30% to 40%. Fig. 5b shows how the final elastic and plastic vertical deformations of the track specimen vary depending on the amount of rubber. The figure shows that elastic and plastic vertical deformations increase as more rubber is added to SEAL, and when R_b increases from 30% to 40% this associated rapid increase in vertical deformation (settlement) corroborates with the severely increased vibration observed in the specimen with SEAL40. It is easy to understand that more rubber will cause more elastic strain as rubber is a visco-elastic material. On the other hand, as more rubber is added in SEAL, the mixture tends to present an increasingly looser condition under the same compaction effort, meaning that the mixture has a larger void space within the granular assembly (Indraratna et al. 2018b, Tawk et al. 2020). This will then enable further compaction under continuously dynamic loading, hence causing a higher plastic deformation.

Compared to the test specimen tested here with conventional subballast materials and the specimen tested under the same loading conditions by Navaratnarajah et al. (2018), the specimen with a SEAL matrix having $R_b \leq 10\%$ has an acceptable settlement (7.2-11 mm) comparing to the settlement of traditional track (5.3-13 mm) (Figs. 3a & 5b). Moreover, less lateral dilation is found for the specimen with $R_b \geq 10\%$ (Fig. 4a). Furthermore, the elastic deformation of 1.52 mm for the specimen with SEAL10 is comparable to a traditional track (Fig. 5b) indicating an acceptable level of vibration. This result also suggests that $R_b = 10\%$ is a proper rate to add into SEAL to ensure the track will have acceptable settlement and less lateral dilation than a traditional track without experiencing greater vertical vibration.

2.3 Energy absorbing property and ballast degradation

Fig. 6 shows that the hysteretic loop of the track specimen at the end of each test varies according to the amount of rubber added. The hysteretic loop of the traditional track specimen is similar to the specimen with SEAL0, albeit with less permanent vertical strain. Note that as more rubber is added to the SEAL matrix, the hysteretic loop of the track specimen expands and shifts to the right, and when R_b increases to 40%, the subsequent increase in the area of the hysteretic loop is substantial. This further proves how the addition of rubber increases the permanent and elastic strain. Moreover, this increase in the loop area also indicates a higher dissipated energy. This has been further elaborated through Fig. 7 where the elastic energy density ($E_{elastic}$) and the dissipated energy density (E_d) of the track specimen at the end of each test are presented.

The dissipated energy density can be represented through the area of the hysteretic loop, whereas the elastic energy density refers to the area below the unloading line for each loading cycle (Qi and Indraratna 2020), as shown in Fig. 7. When R_b increases from 0 to 20%, both $E_{elastic}$ and E_d increase, albeit this increase in dissipated energy is more pronounced (Fig. 7). However, while the $E_{elastic}$ and E_d of the track specimens having SEAL20 and SEAL30 are similar, the track specimen with SEAL40 experienced a sharp increase in $E_{elastic}$ and E_d. This indicates that the skeleton of the SEAL40 matrix is now controlled by the rubber particles which induce a rubber-like behaviour, i.e. a large elastic strain and high compressibility due to larger voids between particles (Indraratna et al. 2020, Tawk et al. 2020). The sum of elastic energy and dissipated energy gives the total amount of absorbed energy by the track substructure. It is therefore easy to conclude that as more rubber is added to SEAL, more energy is absorbed by the track specimen.

While this increase in dissipated energy may result in more energy being consumed by plastic deformation and/or particle breakage (Qi and Indraratna 2020), using SEAL with a higher R_b may not be a favourable outcome. To investigate this possibility further, ballast particles directly beneath the sleeper were collected and sieved after each test to obtain the particle size distribution curves, and the ballast breakage index (BBI) was adopted in this study to evaluate ballast breakage for each test. The value of BBI can be calculated based on the ballast grading curves before and after testing, as initially proposed by Indraratna et al. (2005). The definition of BBI is shown in Fig. 8a, and the BBI obtained after each test is shown in Fig. 8b. Basically, when 10% rubber is added to the SEAL matrix the BBI decreased by almost 60%, but when more rubber is added to SEAL there is no further improvement, which suggests that 10% rubber in SEAL is sufficient to mitigate ballast degradation. Note also that the BBI of the traditional track specimen is similar to the test specimen having SEAL0.

The test results of BBI in Fig. 8b show that the more dissipated energy induced by adding rubber does not result in a higher particle breakage, it actually induces greater plastic deformation, as shown in Fig. 5b. This further indicates that the addition of rubber could reduce ballast breakage by enabling more energy to be consumed by plastic deformation. The ideal percentage of rubber in SEAL is expected to reduce ballast breakage without inducing extensive deformation, in comparison to traditional track materials. Therefore, 10% rubber is the recommended amount for a SEAL matrix in terms of ballast degradation and deformation.

2.4 Track modulus and damping capacity

The stiffness and damping properties are the key parameters governing the dynamic performance of rail track (e.g. vibration, deformation and energy dissipation). The track modulus (K) is commonly used to indicate the vertical stiffness of a track supporting system that includes the faster, the sleepers and track substructure (i.e. ballast, subballast and subgrade), that can be calculated by Equations (1-2), as suggested by Selig and Li (1994):

$$K = \frac{k^{4/3}}{(64EI)^{1/3}} \tag{1}$$

where k is the stiffness of the entire track structure which considering the rail bending stiffness EI, it can be obtained by:

$$k = \frac{q}{\delta} \tag{2}$$

where q is the per unit length vertical supporting stress provided by the track component, and δ is the vertical track deflection. As the track stiffness based on overall vertical deformation is directly influenced by the entire substructure assembly, it is assumed that the calculated value and the proposed relationship for track modulus in this particular study will be suitable for a track substructure that is relatively stiff (e.g. well-compacted ballast interlocked with concrete ties, stiff E-type clip fastener system, solid subgrade) as have been described in the section of Materials and Test Program.

Damping refers to the loss of energy within a vibrating or cyclically loaded system. The damping efficiency can be evaluated using the damping ratio (D) which is the ratio of the dissipated energy to the maximum elastic energy stored during one loading cycle. It can be calculated through the hysteretic loop during the cyclic loading, as shown in Fig. 9b.

The track modulus and damping ratio of the track specimen that vary with the loading cycles are shown in Fig. 9(a,b). As the loading cycles evolve, the track modulus increases at the beginning of each test as the test specimens become denser and rapidly stabilise for the remainder of the test. By increasing the amount of rubber in the SEAL matrix the track modulus decreases which is a direct result caused by the increasing vertical strain but with the same the dynamic load amplitude (Fig. 6), and also it is easy to understand because the shear strength of the rubber materials is less than the other two waste materials in the SEAL mixture (i.e. SFS and CW) (Qi et al. 2019a). Compared to traditional track materials, all the test specimens other than that with SEAL0 have a lower track modulus. A higher track modulus (i.e. track stiffness) always helps to ensure the track has less vibration and deformation, but this may induce a higher interaction force between the sleeper and the ballast due to load concentration (Indraratna et al. 2017). Therefore, it is better for a track foundation with a SEAL matrix (i.e. SEAL10) to have a reasonable comparable track modulus with the traditional track rather than have a much higher or lower value.

The track modulus at the end of each test is shown in Fig. 9c after each test; the figure shows there is an exponential relationship between K and $R_b\%$ with a high regression coefficient of $R^2 = 0.94$:

$$K^* = \alpha_1 e^{\alpha_2 (R_b + 0.1)} \quad (3)$$

where α_1 and α_2 are the fitting coefficients whose values are shown in Fig. 9c.

Note that the test specimen with SEAL0 has a similar damping ratio to the traditional track specimen, but as R_b in the SEAL matrix increases the damping ratio also increases, i.e. a higher energy dissipation efficiency (Fig. 9b). This indicates that as more rubber is added, more energy is dissipated through permanent deformation or/and particle breakage rather than in the form of elastic energy. This is also shown in Fig. 7 where the dissipated energy density gradually exceeds the elastic energy density and dominates as R_b increases.

Track vibration is a complex phenomenon sourced from the moving loads of the train and its propagation depends mainly on the track stiffness and the damping effect of the track substructure. This damping ratio however, is only a relative ratio that reflects the relationship between the dissipated energy and elastic energy rather than directly showing the damping effect of the test specimen. The damping effect of a system that will slow the vibration when subjected to dynamic loading can be evaluated by utilising the viscous damping coefficient (C). This is a theoretical parameter that can explain how the energy dissipation due to friction can slow the motion of the system under dynamic loading (Escalante-Martínez et al. 2016). The viscous damping coefficient (C) strongly depends on the shear modulus and damping ratio of a system, and it can be obtained by using the following equations:

$$C = C_c \times D \tag{4}$$

$$C_c = 2\sqrt{Km} \tag{5}$$

where C_c is the critical damping coefficient and m is the unit mass of the material in the system being considered.

The viscous damping coefficient (C) for each track specimen obtained at the end of the test is shown in Fig. 9c. Basically, it increases as R_b increases to 10% and then decreases as more rubber is added into the SEAL mixture, which suggests that SEAL with 10% rubber can act as a damping cushion in the rail foundation to slow the dynamic vibration. Moreover, an empirical relationship between C and R_b% can be obtained as shown by Equation (6), with a reasonably high coefficient of determination $R^2 = 0.92$.

$$C^* = \beta_1 (R_b)^2 + \beta_2 R_b + \beta_3 \tag{6}$$

where $\beta_{1,2,3}$ are the fitting coefficients whose values are shown in Fig. 9c.

2.5 Dynamic amplification factor

Under dynamic loading conditions, the actual stress imparted by the track foundation is usually higher than the applied load. One of the main functions of the subballast layer is to distribute the load and reduce the stress being transmitted to other layers. To investigate how the incorporation of SEAL will influence the interface stress between each layer of track substructure, the measured stress at the interface of each test specimen is shown in Fig. 10a. Note here that the measured stress at the interface decreases along the depth of the test specimen. At the interface of the same layer, the track specimen with SEAL10 has the lowest stress while the specimen with SEAL40 has the highest, and the stress at the interface of the traditional track specimen is higher than the specimen with SEAL10 but lower than the other test specimens.

The dynamic amplification factor (DAF) is used to evaluate the dynamic loading in this study. It is a dimensionless parameter. It is the ratio between the maximum stress caused by the dynamic or cyclic load to the maximum deviator stress applied to the structure, and can be obtained via Equation (7), as suggested by Sun et al. (2016):

$$\mathrm{DAF}=q_{d,max}/q_{max,cyc} \tag{7}$$

where $q_{d,max}$ is the peak dynamic deviator stress measured during the cyclic loading test, and $q_{max,cyc}$ is the applied maximum deviator stress.

The DAF of the test specimen that varies with the amount of rubber is shown in Fig. 10b. This figure shows that DAF decreases from the top layer of ballast to the bottom layer of subgrade as the stress is distributed alongside the depth. When 10% RC is added in the SEAL matrix, DAF decreases slightly from 1.25 to 1.1 and then increases as R_b increases. Note that the DAF on top of ballast of the specimen with SEAL40 is more than double that of the specimen with SEAL10, and the interface stress on top of the ballast has doubled compared to the pressure applied due to the dynamic effect. The additional stress generated under the dynamic environment depends mainly on the lateral confinement, the loading frequency, the track stiffness and damping effect, and the energy absorbing capacity of the track substructure (Esveld and Esveld 2001). A track substructure with a relatively high track stiffness, low damping coefficient, and low energy absorbing capacity that is subjected to a high lateral confining pressure and high loading frequency will generate a high DAF, and this extensive additional stress may result in high deformation and ballast breakage. Given that the lateral confinement and loading frequency are controlled the same during testing, the DAF for the track specimen in this study is influenced by a combination of track stiffness, damping coefficient, and energy absorbing capacity. Furthermore, since the track specimen with SEAL10 has the lowest DAF, it is recommended that the optimal percentage of rubber should be 10% in a SEAL matrix when the dynamic amplification effect is considered.

3. Predicted dynamic response of rail with SEAL incorporated track

To investigate how SEAL will affect the dynamic response (vertical displacement and acceleration) of rail in field conditions, a simple track dynamic model considering a platoon of moving line loads is adopted in this study (Fig. 11). The rail is considered to be a Bernoulli-Euler beam resting on a viscoelastic foundation that incorporates SEAL. This viscoelastic foundation is equivalent to a spring and dashpot system (Fig. 11) as the track foundation is simplified as a complete system during prismoidal triaxial testing to measure the track modulus and viscous damping coefficient. Assuming the rail deflection is u in the vertical direction, the moving load is travelling in x direction (horizontally along the track), and the time is t, the origin of the coordinate system is set at the middle of the distribution of the last moving load. The common governing equation of a Bernoulli-Euler beam on a viscoelastic foundation is:

$$EIu^{(4)}(x) + K^*u + C^*\dot{u}(t) + m\ddot{u}(t) = F(x,t) \quad (8)$$

where EI is the bending stiffness of the rail, K^* and C^* are the stiffness and the viscous damping coefficient of the track substructure that varies with the percentage of rubber in SEAL, as denoted by Equations (3) and (6), respectively. Assuming the length of the rail is infinite, the boundary conditions are: $u(\pm\infty) = 0; \lim_{x\to\pm\infty} u^{(j)}\left(x^{j}\right) = 0, j = 1, 2, 3, 4$.

$F(x, t)$ is the external dynamic load (a platoon of uniform moving line loads with uniform distributions), as represented by Equation (9) (Sun and Luo 2008):

$$F(x,t) = \sum_{n=1}^{n} P\exp\,(i\Omega t)(2r)^{-1} H(r - \left| x - vt - \sum_{n=1}^{n} l_n \right|) \tag{9}$$

where *i* is a unit imaginary number. Each load is $2r$ long and n is the number of moving loads, and P and Ω are the amplitude and frequency of the jth load, respectively. l is the space between the middle point of two adjacent moving loads. The moving load is travelling at a speed of v, and $H(\cdot)$ is the unit Heaviside step function defined as:

$$H(x - x_0) = \begin{cases} 0 & \text{for } x < x_0 \\ \frac{1}{2} & \text{for } x = x_0 \\ 1 & \text{for } x > x_0 \end{cases} \tag{10}$$

Applying the Fourier transform to Equation (8) and rearranging it gives:

$$\tilde{u}(\xi, \omega) = \frac{\tilde{F}(\xi, \omega)}{EI\xi^4 + K^* + iC^*\omega - m\omega^2} \tag{11}$$

Applying the inverse Fourier transform to Equation (11) gives an integral representation of the steady-state dynamic displacement of the beam in the time domain:

$$u(x,t) = (2\pi)^{-2} \int_{-\infty}^{\infty} \int_{-\infty}^{\infty} \frac{\tilde{F}(\xi, \omega)\exp\,[i(\xi x + \omega t)]}{EI\xi^4 + K^* + iC^*\omega - m\omega^2}\, d\xi d\omega \tag{12}$$

Applying the Fourier transform to Equation (9):

$$\tilde{F}(\xi,\omega) = \int_{-\infty}^{\infty}\int_{-\infty}^{\infty}\sum_{n=1}^{n} P\exp\,(i\Omega t)(2r)^{-1}H(r - \left|x - vt - \sum_{n=1}^{n} l_n\right|)\exp\,[-i(\xi x + \omega t)]dxdt \tag{13}$$

Note that:

$$\int_{-\infty}^{\infty}(2r)^{-1}H(r - \left|x - vt - \sum_{n=1}^{n} l_n\right|)\exp\,[-i(\xi x)dx$$
$$= \int_{vt+\sum_{n=1}^{n} l_n - r_0}^{vt+\sum_{n=1}^{n} l_n + r_0} \frac{\exp\,(-i\xi x)}{2r_0}dx \tag{14}$$
$$= \frac{sinr\xi}{r\xi}\exp\,[-i\xi(vt + \sum_{n=1}^{n} l_n)]$$

$$\int_{-\infty}^{\infty}\exp[-i(\omega + v\xi - \Omega)t]\,dt = 2\pi\delta(\omega + v\xi - \Omega) \tag{15}$$

where $\delta(x)$ is the Dirac function.

Substituting Equations (14-15) into Equation (13) gives:

$$\tilde{F}(\xi,\omega) = \sum_{n=1}^{n} 2\pi P\exp\,(-i\xi\sum_{n=1}^{n} l_n)(r\xi)^{-1}\sin\,(r\xi)\,(\omega + v\xi - \Omega) \tag{16}$$

Substituting Equation (16) into Equation (12) gives the vertical displacement of the rail:

$$u(x,t) = \sum_{j=1}^{J} \frac{\bar{P}}{2\pi} \exp{(i\Omega t)} \times \int_{-\infty}^{\infty} \frac{EI \sin(r\xi) \exp[i\xi(x-vt)] \exp{(-i\xi \sum_{n=1}^{n} l_n)}}{r\xi[EI\xi^4 + K^* + iC^*(\Omega - v\xi) - m\omega(\Omega - v\xi)^2)} d\xi \tag{17}$$

The vertical acceleration of the beam can then be obtained by differentiating Equation (17):

$$\text{Acceleration:} \quad \ddot{u}_t(x,t) = \sum_{n=1}^{n} \frac{\bar{P}}{2\pi} \exp{(i\Omega t)} \times \int_{-\infty}^{\infty} \frac{EI(\Omega - v\xi)^2 \sin(r\xi) \exp[i\xi(x-vt)] \exp{(-i\xi \sum_{n=1}^{n} l_n)}}{r\xi[EI\xi^4 + K^* + iC^*(\Omega - v\xi) - m\omega(\Omega - v\xi)^2)} d\xi \tag{18}$$

All the parameters used for numerical computing this track dynamic model are listed in Table 1. The listed loading condition and the parameters of the track foundation simulate field loading conditions. P=50 kN and $\Omega = 15$ Hz are the amplitude of the load and the loading frequency, respectively, used to simulate a train with a 25-tonne axle load running at 115 km/h. The values of K and C for each track having different SEAL matrices are obtained from the large scale prismoidal triaxial tests. The length of the load distribution is $2r = 15.75\ m$ and the space between the two middle points of two adjacent loads is assumed to be $l = 18.75\ m$; this simulates standard suburban carriage stock in New South Wales, Australia (Punetha et al. 2020).

The dynamic responses (i.e. displacement and acceleration) of a rail subjected to a single moving load with varying viscous damping coefficients and track stiffness in the track substructure are shown in Fig. 12 and Fig. 13, respectively. The observation point is at $x = 0$, which is the point of origin of the coordinate system, and where $t = 0$ means the moving load is passing through the observation point. Both negative and positive values can be observed for the rail dynamic response, indicating the rail experiences tensile and compressive stresses as the moving load passes by. When the magnitude of the viscous damping coefficient is changed while all the other parameters are the same, there is a marginal change in displacement and acceleration as C increases from 10^4 to $10^5\ Ns/m^2$, and a large reduction (50-80%) when C increases from 10^5 to $10^6\ Ns/m^2$ and then to $10^7\ Ns/m^2$. Moreover, peak displacement and acceleration are not sensitive to changes in the track stiffness from 10^5 to $10^6\ N/m^2$ but they decrease significantly when the track stiffness varies between 10^6 to $10^9\ N/m^2$. Furthermore, a reduction in track stiffness induces vertical deflection to takes longer to recover (Fig. 13a). Given that the track stiffness and viscous damping coefficient of track substructure will generally vary between $10^5 \leq C \leq 10^7\ N/m^2$ and $10^6 \leq K \leq 10^9\ N/m^2$, the damping property and track stiffness of the track substructure are the two key factors that influence rail deformation and vibration.

Because changing the amount of rubber in the subballast layer changes the damping property and track stiffness, a plot of the dynamic response of rail that varies with the amount of rubber shows a combination change of the damping property and track stiffness, as shown in Fig. 14. The model prediction shows that when increasing the amount of rubber in SEAL, a rail experiences higher displacement and acceleration, which indicates that more rubber can generate more deformation and vibration for the rail track. This agrees with the laboratory test results where more rubber generates more vertical deformation (shown earlier in Fig. 3) and more elastic energy (see Fig. 7). Moreover, when the percentage of rubber in SEAL increases to 40% the subsequently sharp jump in displacement and acceleration is almost 2-3 times greater than without rubber. This matches the laboratory observation that the track with SEAL40 collapsed with severe vibration and displacement. Compared to the traditional track, rail tracks with SEAL0 and SEAL10 have similar or even less vertical deflection and acceleration.

To obtain a further space-time overview of how the percentage of rubber in SEAL affects the vertical vibration of rail, a three-dimensional view of the acceleration of rail by applying a platoon of ten moving loads (i.e. $n = 10$) is shown in Fig. 15. The peak acceleration occurs almost at the point of origin of the coordinate system. It is noted that the amplitude of acceleration increases as more rubber is added to the track foundation. The peak acceleration of track with SEAL40 is almost 60% greater than with SEAL0, whereas acceleration with SEAL10 is comparable to a traditional track, and this is in line with the laboratory observations.

Overall, the track dynamic model further validates how the percentage of rubber crumbs used in the subballast layer will affect the dynamic response of track, such that more rubber generates more settlement and vibration, while the settlement and vibration of the track with SEAL10 is comparable to traditional track. Furthermore, utilising SEAL10 leads to less lateral dilation, less ballast degradation, and less dynamic pressure at the interface of the substructure. Therefore, 10% rubber is recommended to be included in SEAL to replace traditional subballast materials.

4. Limitations of the study

Apart from the properties of the substructure materials, track dynamic response is also influenced by other parameters such as the excitation frequency, varied axle loads from different rolling stock generating a wider array of cyclic stress ratios as well as the structural assembly of track and the type of gauge (i.e. geometry and ballast-sleeper assemblies). The individual roles of all these influential factors could not be considered within the scope of this single study. Consequently, the contents of this paper are subjected to certain limitations within its current scope in relation to the following simplifications and assumptions.

(i) The computed track modulus is based on the assumption of a relatively stiff track substructure consisting of well-compacted ballast and sub-ballast overlying a solid subgrade; the analysis may deviate from accuracy if the substructure layers are considerably softer or compressible.

(ii) The laboratory investigation and the track dynamic model were specifically focused on examining the influence of rubber contents in the energy absorbing mixtures on the track dynamic response, while all other contributory factors (e.g. track geometry and structure, loading conditions, ballast and subgrade characteristics) were kept unchanged. Indeed, the track response will be different if other parameters are also varied, for instance if the track construction materials were to be changed.

(iii) Only one value of loading frequency (15 Hz) was used in the current study that would corroborate with the range of 80-110 km/h speeds for heavy haul trains in Australia depending on the type of track gauge and the bogey spacing of freight trains. Naturally, either much smaller or much greater frequencies for the same applied cyclic load will generate varied track dynamics.

5. Conclusions

In this paper, a synthetic energy absorbing layer (SEAL) was proposed to replace traditional subballast material. The performance of track specimens with SEAL was examined through large-scale prismoidal triaxial tests under cyclic loading by changing the amount of rubber in the SEAL matrix. It was revealed that the amount of RC within the SEAL matrix had a significant influence on the dynamic response (deformation, ballast degradation, track modulus, damping ratio, vibration, stress distribution, and energy absorbing capacity) of the rail foundation. On this basis a track dynamic model was developed to better investigate track performance when SEAL was used. The following conclusions can be drawn from this study:

(1) When the amount of rubber in the SEAL matrix was increased the permanent and elastic vertical displacement of the track specimen increased, but its lateral dilation decreased. When the rubber content in SEAL was $\geq 20\%$, lateral deformation fluctuated as compression and dilation appeared alternately. The test specimen with SEAL40 reached plastic collapse with extensive settlement and excessive vibration at around 1500 loading cycles, whereas all the other specimens achieved plastic shakedown before the test ended.

(2) The addition of rubber in SEAL increased the total energy absorbing capacity of the track specimen and mitigated ballast breakage. When 10% of rubber was added to SEAL, the BBI decreased by almost 60%, but when more rubber was added there was no further benefit. This implies that for each type and gradation of granular material, an optimum rubber content exists beyond which the returns are marginal.

(3) Adding resilient rubber to the SEAL matrix reduced the track modulus and increased the damping ratio of the track specimen (i.e. the efficiency to dissipate energy). The viscous damping coefficient which reflected its ability to reduce motion increased as 10% rubber was included, after which it decreased again. These results imply that the damping coefficient of the SEAL is directly related to the optimum rubber content. While it was evaluated at 10% for the material tested herein, for significantly different types of granular soils and rockfills the optimum rubber content may deviate from 10%.

(4) The pressure at the interface and DAF decreased along with the depth of the track foundation. The test specimen with SEAL10 had the lowest pressure and DAF at the interface of each layer, whereas the interface pressure and DAF increased as rubber contents increased beyond 10%.

(5) A dynamic track model was developed to investigate the dynamic response of rail tracks incorporating the SEAL matrix. It was found that the dynamic response of rail (deflection and acceleration) was mainly affected by the track modulus and damping property, both of which were governed by changing the percentage of rubber in SEAL. While the addition of rubber increased the vertical deflection and acceleration of the track, the use of SEAL10 would still ensure an acceptable dynamic response.

(6) Compared to the traditional track specimens, adding 10% rubber in SEAL reduced lateral dilation, ballast degradation, and stresses developed at the interface, while maintaining an acceptable level of vertical deformation and vibration. On this basis SEAL10 can be recommended to be a promising option for rubber-blended capping or subballast materials to replace traditional subballast in rail tracks.

Data Availability statement

Some or all data, models, or code that support the findings of this study are available from the corresponding author upon reasonable request.

Acknowledgements

The authors would like to acknowledge the financial support provided by the Australian Research Council Discovery Project (ARC-DP; project ID: DP180101916). The assistance provided by industry (ASMS, South 32, and Tire Crumb Australia) in relation to the procurement of material used in this study is gratefully acknowledged.

References

Escalante-Martínez, J., Gómez-Aguilar, J., Calderón-Ramón, C., Morales-Mendoza, L., Cruz-Orduna, I. and Laguna-Camacho, J. (2016). "Experimental evaluation of viscous damping coefficient in the fractional underdamped oscillator." *Advances in Mechanical Engineering* 8(4): 1687814016643068.

Esmaeili, M., Aela, P. and Hosseini, A. (2017). "Experimental assessment of cyclic behavior of sand-fouled ballast mixed with tire derived aggregates." *Soil Dynamics and Earthquake Engineering* 98: 1-11.

Esveld, C. and Esveld, C. (2001). Modern railway track, MRT-productions Zaltbommel, Netherlands.

Fathali, M., Esmaeili, M. and Nejad, F. M. (2019). "Influence of tire-derived aggregates mixed with ballast on ground-borne vibrations." *Journal of Modern Transportation* 27(4): 355-363.

Fernandes, G., Palmeira, E. M. and Gomes, R. C. (2008). "Performance of geosynthetic-reinforced alternative sub-ballast material in a railway track." *Geosynthetics International* 15(5): 311-321.

Fernández, P. M., Signes, C. H., Sanchís, I. V., Mira, D. P. and Franco, R. I. (2018). "Real scale evaluation of vibration mitigation of sub-ballast layers with added tyre-derived aggregate." *Construction and Building Materials* 169: 335-346.

Gong, H., Song, W., Huang, B., Shu, X., Han, B., Wu, H. and Zou, J. (2019). "Direct shear properties of railway ballast mixed with tire derived aggregates: Experimental and numerical investigations." *Construction and Building Materials* 200: 465-473.

Indraratna, B., Ferreira, F. B., Qi, Y. and Ngo, T. N. (2018a). "Application of geoinclusions for sustainable rail infrastructure under increased axle loads and higher speeds." *Innovative Infrastructure Solutions* 3(1): 69.

Indraratna, B., Lackenby, J. and Christie, D. (2005). "Effect of confining pressure on the degradation of ballast under cyclic loading." *Geotechnique* 55(4): 325-328.

Indraratna, B. and Nimbalkar, S. (2013). "Stress-strain degradation response of railway ballast stabilized with geosynthetics." *Journal of geotechnical and geoenvironmental engineering* 139(5): 684-700.

Indraratna, B., Qi, Y. and Heitor, A. (2018b). "Evaluating the properties of mixtures of steel furnace slag, coal wash, and rubber crumbs used as subballast." *Journal of Materials in Civil Engineering* 30(1): 04017251.

Indraratna, B., Qi, Y., Ngo, T. N., Rujikiatkamjorn, C., Neville, T., Ferreira, F. B. and Shahkolahi, A. (2019). "Use of geogrids and recycled rubber in railroad infrastructure for enhanced performance." *Geosciences* 9(1): 30.

Indraratna, B., Qi, Y., Tawk, M., Heitor, A., Rujikiatkamjorn, C. and Navaratnarajah, S. K. (2020). "Advances in Ground Improvement Using Waste Materials for Transportation Infrastructure." *Proceedings of the Institution of Civil Engineers-Ground Improvement*: 1-44.

Indraratna, B., Sun, Q. and Grant, J. (2017). "Behaviour of subballast reinforced with used tyre and potential application in rail tracks." *Transportation Geotechnics* 12: 26-36.

Indraratna, B., Sun, Q., Heitor, A. and Grant, J. (2018c). "Performance of rubber tire-confined capping layer under cyclic loading for railroad conditions." *Journal of Materials in Civil Engineering* 30(3): 06017021.

Jayasuriya, C., Indraratna, B. and Ngo, T. N. (2019). "Experimental study to examine the role of under sleeper pads for improved performance of ballast under cyclic loading." *Transportation Geotechnics* 19: 61-73.

Kaewunruen, S., Aikawa, A. and Remennikov, A. M. (2017). "Vibration attenuation at rail joints through under sleeper pads." *Procedia engineering* 189: 193-198.

Kaewunruen, S. and Remennikov, A. M. (2016). "Current state of practice in railway track vibration isolation: an Australian overview." *Australian Journal of Civil Engineering* 14(1): 63-71.

Lackenby, J., Indraratna, B., McDowell, G. and Christie, D. (2007). "Effect of confining pressure on ballast degradation and deformation under cyclic triaxial loading." *Géotechnique* 57(6): 527-536.

Lakušić, S., Ahac, M. and Haladin, I. (2010). Experimental investigation of railway track with under sleeper pad. 10th Slovenian road and transportation congress.

Li, D. and Selig, E. T. (1995). "Wheel/track dynamic interaction: track substructure perspective." *Vehicle System Dynamics* 24(sup1): 183-196.

Navaratnarajah, S. K. and Indraratna, B. (2017). "Use of rubber mats to improve the deformation and degradation behavior of rail ballast under cyclic loading." *Journal of geotechnical and geoenvironmental engineering* 143(6): 04017015.

Navaratnarajah, S. K., Indraratna, B. and Ngo, N. T. (2018). "Influence of under sleeper pads on ballast behavior under cyclic loading: experimental and numerical studies." *Journal of Geotechnical and Geoenvironmental Engineering* 144(9): 04018068.

Ngo, T. N., Indraratna, B. and Rujikiatkamjorn, C. (2019). "Improved performance of ballasted tracks under impact loading by recycled rubber mats." *Transportation Geotechnics* 20: 100239.

Nimbalkar, S., Indraratna, B., Dash, S. K. and Christie, D. (2012). "Improved performance of railway ballast under impact loads using shock mats." *Journal of geotechnical and geoenvironmental engineering* 138(3): 281-294.

Punetha, P., Nimbalkar, S. and Khabbaz, H. (2020). "Analytical Evaluation of Ballasted Track Substructure Response under Repeated Train Loads." *International Journal of Geomechanics* 20(7): 04020093.

Qi, Y. and Indraratna, B. (2020). "Energy-Based Approach to Assess the Performance of a Granular Matrix Consisting of Recycled Rubber, Steel-Furnace Slag, and Coal Wash." *Journal of Materials in Civil Engineering* 32(7): 04020169.

Qi, Y., Indraratna, B. and Coop, M. R. (2019a). "Predicted behavior of saturated granular waste blended with rubber crumbs." *International Journal of Geomechanics* 19(8): 04019079.

Qi, Y., Indraratna, B., Heitor, A. and Vinod, J. S. (2018a). "Effect of rubber crumbs on the cyclic behavior of steel furnace slag and coal wash mixtures." *Journal of Geotechnical and Geoenvironmental Engineering* 144(2): 04017107.

Qi, Y., Indraratna, B., Heitor, A. and Vinod, J. S. (2019b). "Closure to “Effect of Rubber Crumbs on the Cyclic Behavior of Steel Furnace Slag and Coal Wash Mixtures” by Yujie Qi, Buddhima Indraratna, Ana Heitor, and Jayan S. Vinod." *Journal of Geotechnical and Geoenvironmental Engineering* 145(1): 07018035.

Qi, Y., Indraratna, B. and Vinod, J. S. (2018b). "Behavior of steel furnace slag, coal wash, and rubber crumb mixtures with special relevance to stress–dilatancy relation." *Journal of Materials in Civil Engineering* 30(11): 04018276.

Qi, Y., Indraratna, B. and Vinod, J. S. (2018c). Dynamic Properties of Mixtures of Waste Materials. GeoShanghai International Conference, Springer.

Selig, E. T. and Li, D. (1994). "Track modulus: Its meaning and factors influencing it." *Transportation Research Record*(1470).

Sol-Sánchez, M., Moreno-Navarro, F. and Rubio-Gámez, M. C. (2014). "Viability of using end-of-life tire pads as under sleeper pads in railway." *Construction and Building Materials* 64: 150-156.

Sol-Sánchez, M., Thom, N., Moreno-Navarro, F., Rubio-Gamez, M. and Airey, G. (2015). "A study into the use of crumb rubber in railway ballast." *Construction and Building Materials* 75: 19-24.

Sun, L. and Luo, F. (2008). "Steady-state dynamic response of a Bernoulli–Euler beam on a viscoelastic foundation subject to a platoon of moving dynamic loads." *Journal of Vibration and Acoustics* 130(5): 051002.

Sun, Q. D., Indraratna, B. and Nimbalkar, S. (2016). "Deformation and degradation mechanisms of railway ballast under high frequency cyclic loading." *Journal of Geotechnical and Geoenvironmental Engineering* 142(1): 04015056.

Tatsuoka, F., Tateyama, M., Koseki, J. and Yonezawa, T. (2014). "Geosynthetic-reinforced soil structures for railways in Japan." *Transportation Infrastructure Geotechnology* 1(1): 3-53.

Tawk, M., Qi, Y., Indraratna, B., Rujikiatkamjorn, C. and Heitor, A. (2020). "Behaviour of a Mixture of Coal Wash and Rubber Crumbs under Cyclic Loading." *Journal of Materials in Civil Engineering*.

Toward, M. G., Jiang, J., Dijckmans, A., Coulier, P., Thompson, D. J., Degrande, G., Lombaert, G. and Hussein, M. F. (2014). Mitigation of railway induced vibrations by using subgrade stiffening and wave impeding blocks. 9th International Conference on Structural Dynamics (EURODYN 2014).

Xin, T. and Gao, L. (2011). "Reducing slab track vibration into bridge using elastic materials in high speed railway." *Journal of Sound and Vibration* 330(10): 2237-2248.

Youwai, S. and Bergado, D. T. (2003). "Strength and deformation characteristics of shredded rubber tire sand mixtures." *Canadian geotechnical journal* 40(2): 254-264.

Table list

Table 1 Parameters for SEAL incorporated track

Parameters	SEAL 0	SEAL10	SEAL20	SEAL30	SEAL40	Traditional
P (kN)	50	50	50	50	50	50
EI (N/m^2)	2300	2300	2300	2300	2300	2300
K (N/m^2)	$10.7*10^7$	$6.3*10^7$	$4.8*10^7$	$4.4*10^7$	$1.6*10^7$	$7.1*10^7$
m (kg/m)	2033.58	1999.75	1974.08	1953.41	1935.92	2011.75
C (Ns/ m^2)	$3.46*10^5$	$4.55*10^5$	$3.89*10^5$	$3.59*10^5$	$2.32*10^5$	$3.03*10^5$
Ω (Hz**)**	15	15	15	15	15	15

Figure captions

Fig. 1 Grading curves for ballast, traditional subballast, structural fill, steel furnace slag, coal wash, rubber crumbs, and the SEAL matrix

Fig. 2 (a) Large-scale prismoidal triaxial apparatus with a well-prepared specimen; (b) cross-section view of the 3-layered physical model; (c) cyclic loading conditions

Fig. 3 Deformation responses of the track specimens with different SEAL matrix or traditional materials: (a) vertical displacement, (b) accumulation rate of vertical strain

Fig. 4 (a) Lateral displacement of the track specimens with different SEAL matrix and traditional materials; and accumulation rate of lateral strain of track specimens with (b-1, b-2) SEAL0-SEAL30 and traditional materials, (b-3) SEAL40

Fig. 5 Deformation responses of the track specimens with different SEAL matrix or traditional materials: (a) elastic vertical deformation, and (b) total plastic and elastic deformation

Fig. 6 Hysteretic loops of the track specimen with traditional subballast or SEAL matrix having different rubber contents at the end of each test

Fig. 7 Energy density of the track specimen with SEAL matrix having different rubber contents at the end of each test

Fig. 8 (a) Definition of ballast breakage index (BBI); (b) BBI obtained from each test

Fig. 9 Track modulus and damping ratio of the track specimen with SEAL matrix or traditional subballast materials (a-b) changing with loading cycles, and (c) at the end of each test

Fig. 10 (a) Measured pressure on top of each layer (i.e. ballast, subballast and structural fill) for each test; (b) DAF for track specimen changing with RC contents within SEAL matrix

Fig. 11 A rail track subjected to a platoon of uniform moving line loads

Fig. 12 Dynamic response of rail with changing viscous damping coefficients: (a) displacement and (b) acceleration

Fig. 13 Dynamic response of rail with changing shear stiffness: (a) displacement and (b) acceleration

Fig. 14 Predicted rail dynamic response for traditional track and track incorporated with SEAL (a) displacement and (b) acceleration

Fig. 15 Predicted 3-D view of the acceleration for the track with (a) SEAL0, (b) SEAL10, (c) SEAL20, (d) SEAL30 and (e) SEAL40 and (f) traditional materials

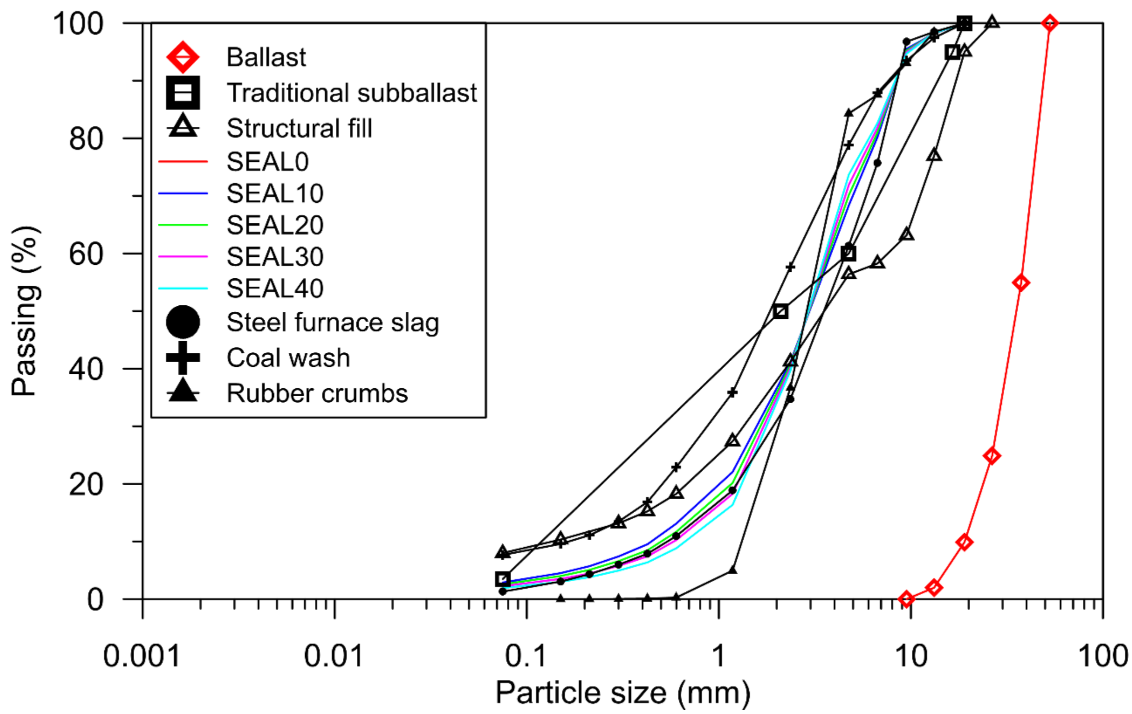

Fig. 1 Grading curves for ballast, traditional subballast, structural fill, steel furnace slag, coal wash, rubber crumbs, and the SEAL matrix

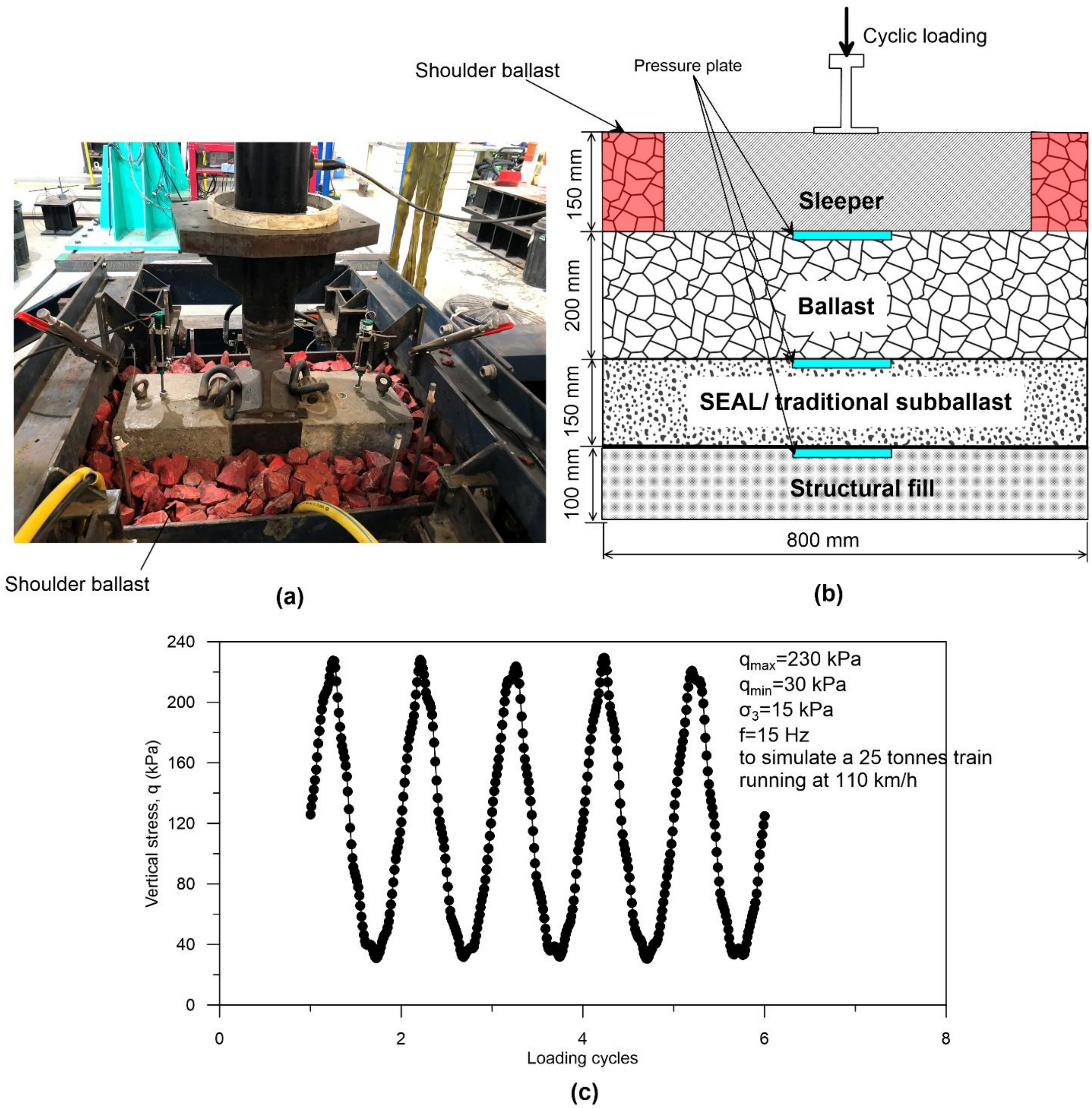

Fig. 2 (a) Large-scale prismoidal triaxial apparatus with a well-prepared specimen; (b) cross-section view of the 3-layered physical model; (c) cyclic loading conditions

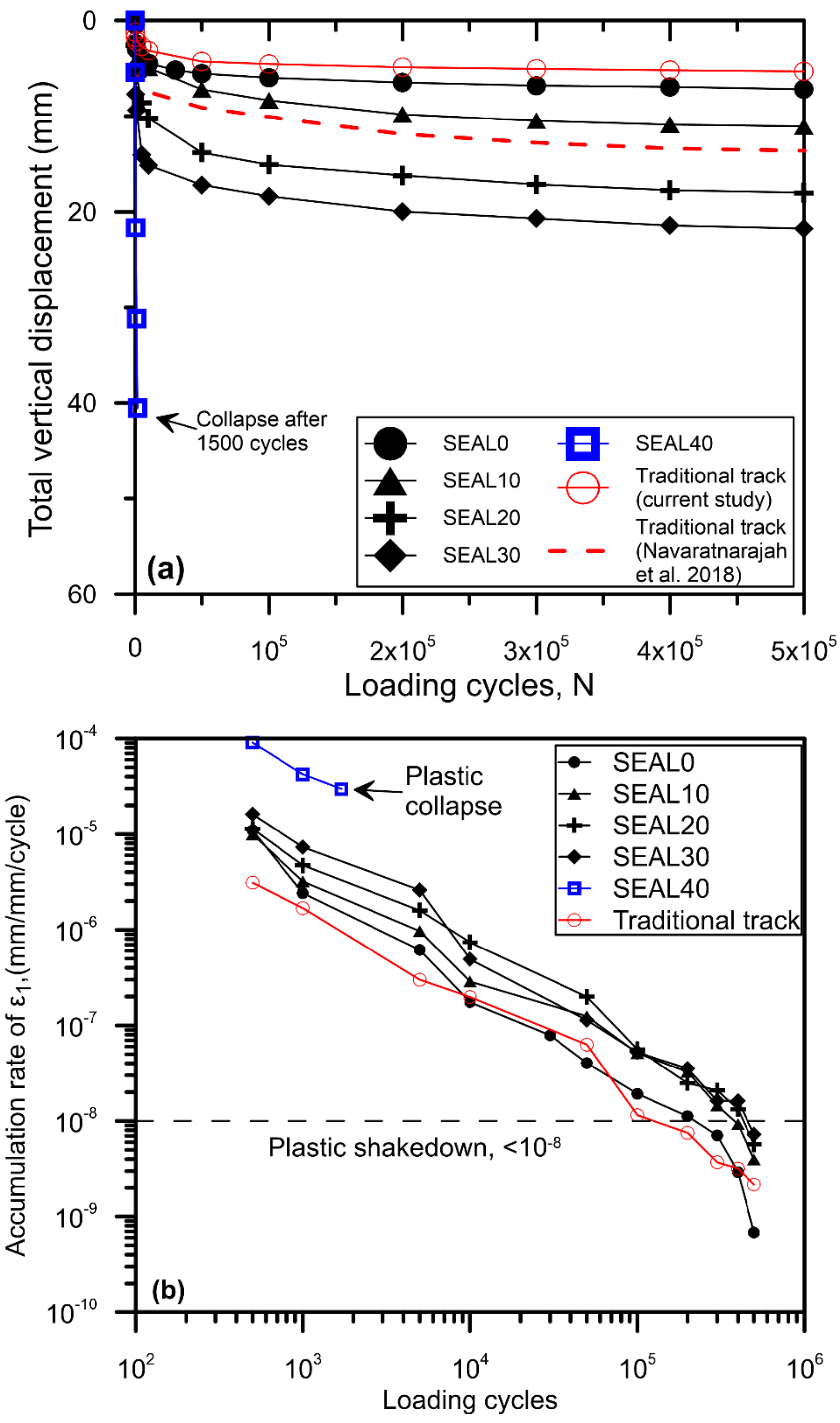

Fig. 3 Deformation responses of the track specimens with different SEAL matrix or traditional materials: (a) vertical displacement, (b) accumulation rate of vertical strain

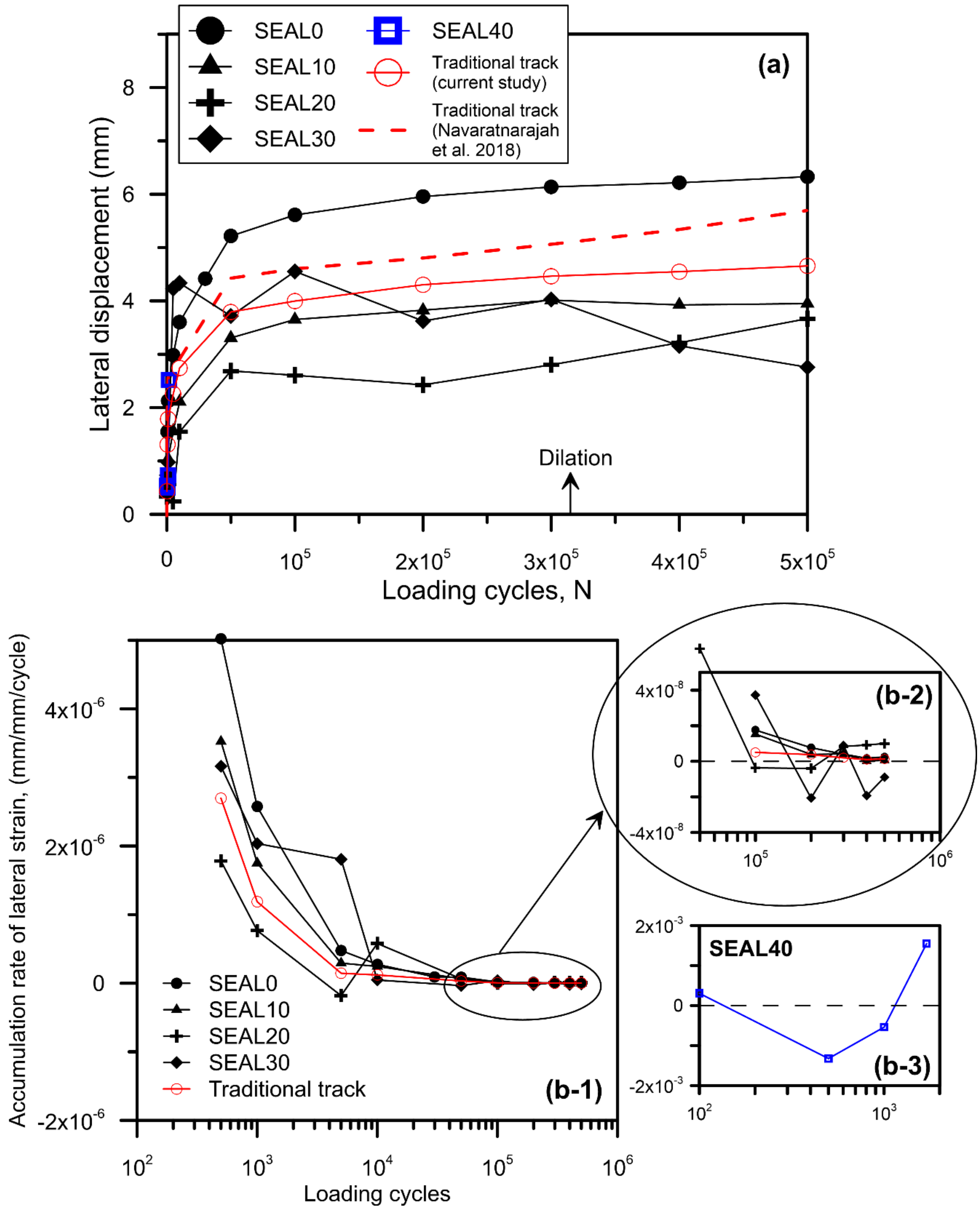

Fig. 4 (a) Lateral displacement of the track specimens with different SEAL matrix and traditional materials; and accumulation rate of lateral strain of track specimens with (b-1, b-2) SEAL0-SEAL30 and traditional materials, (b-3) SEAL40

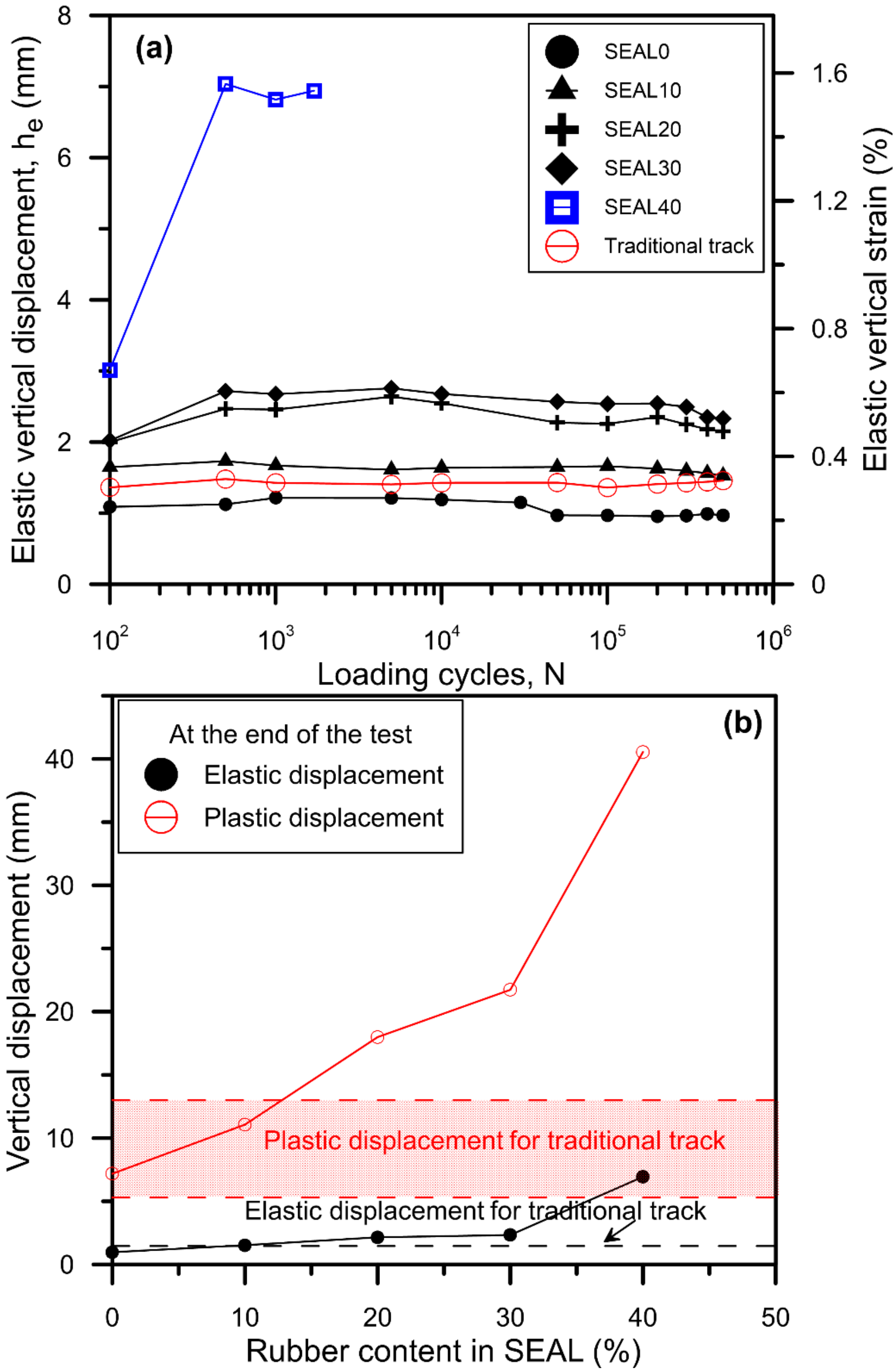

Fig. 5 Deformation responses of the track specimens with different SEAL matrix or traditional materials: (a) elastic vertical deformation, and (b) total plastic and elastic deformation

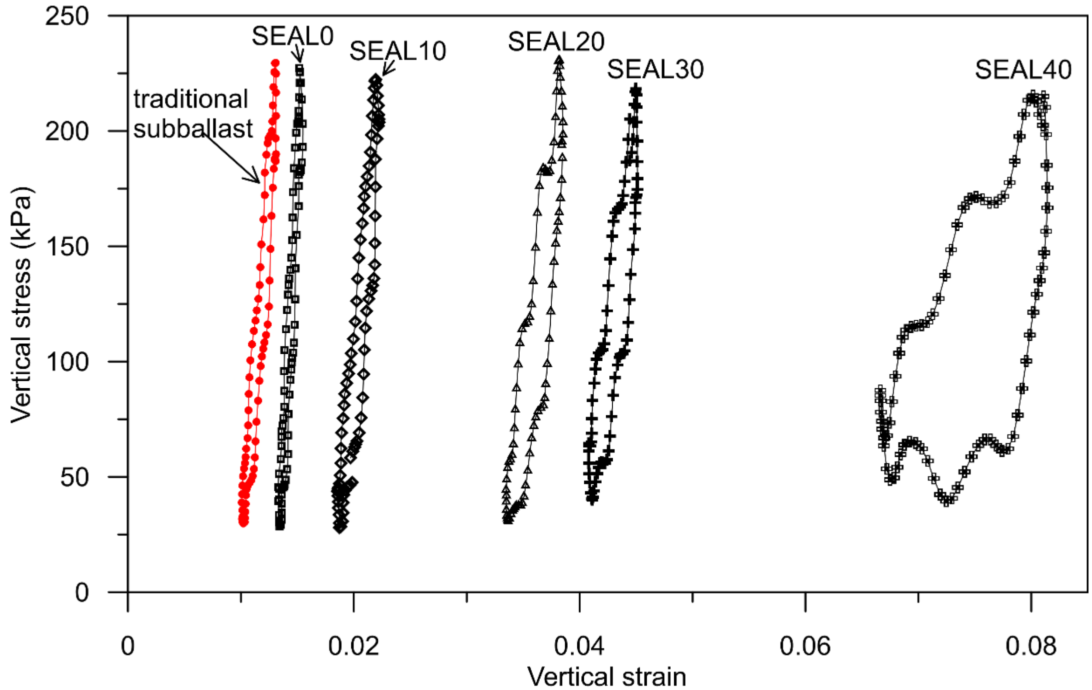

Fig. 6 Hysteretic loops of the track specimen with traditional subballast or SEAL matrix having different rubber contents at the end of each test

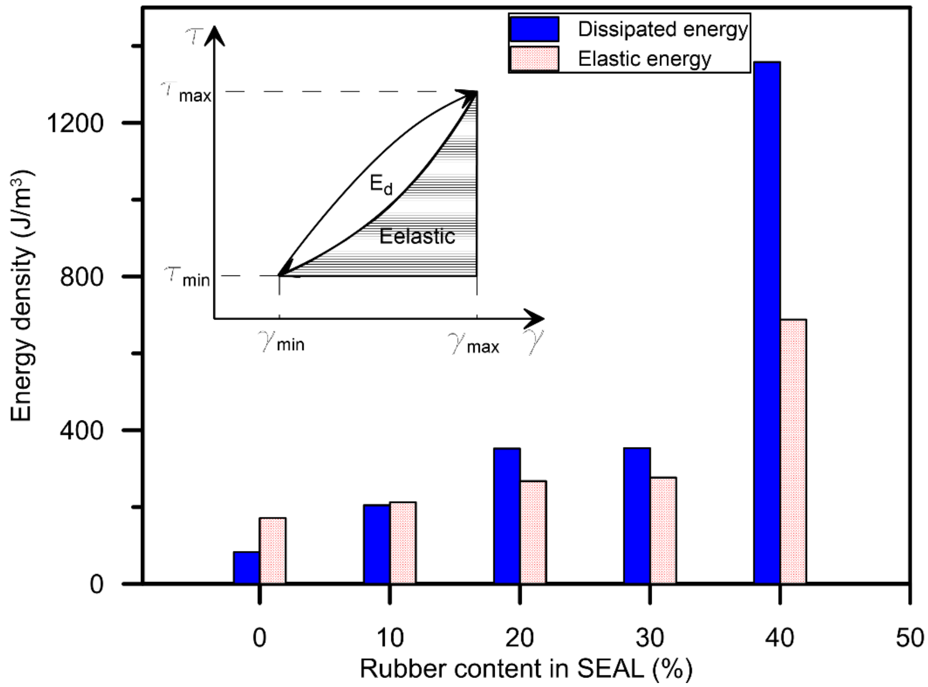

Fig. 7 Energy density of the track specimen with SEAL matrix having different rubber contents at the end of each test

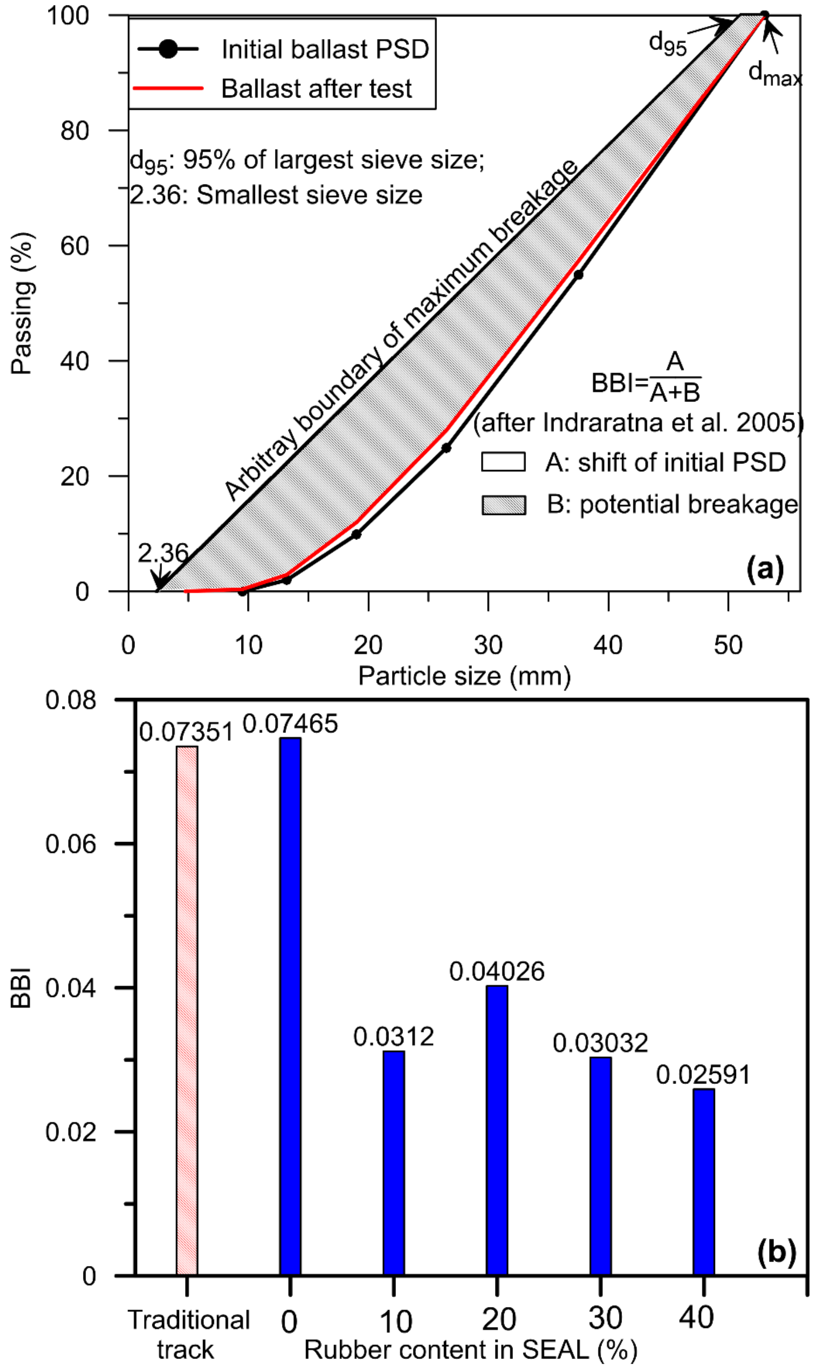

Fig. 8 (a) Definition of ballast breakage index (BBI); (b) BBI obtained from each test

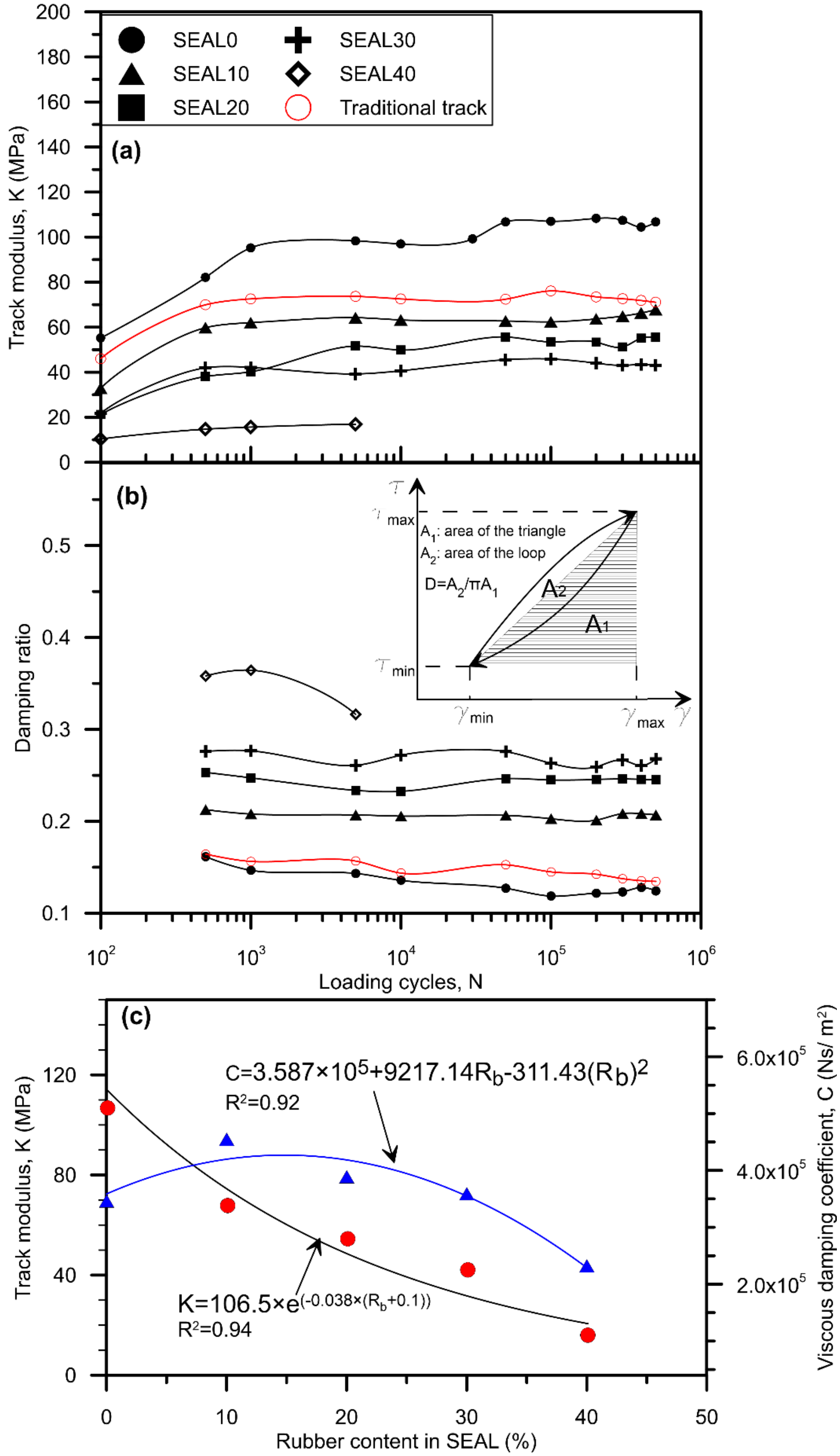

Fig. 9 Track modulus and damping ratio of the track specimen with SEAL matrix or traditional subballast materials (a-b) changing with loading cycles, and (c) at the end of each test

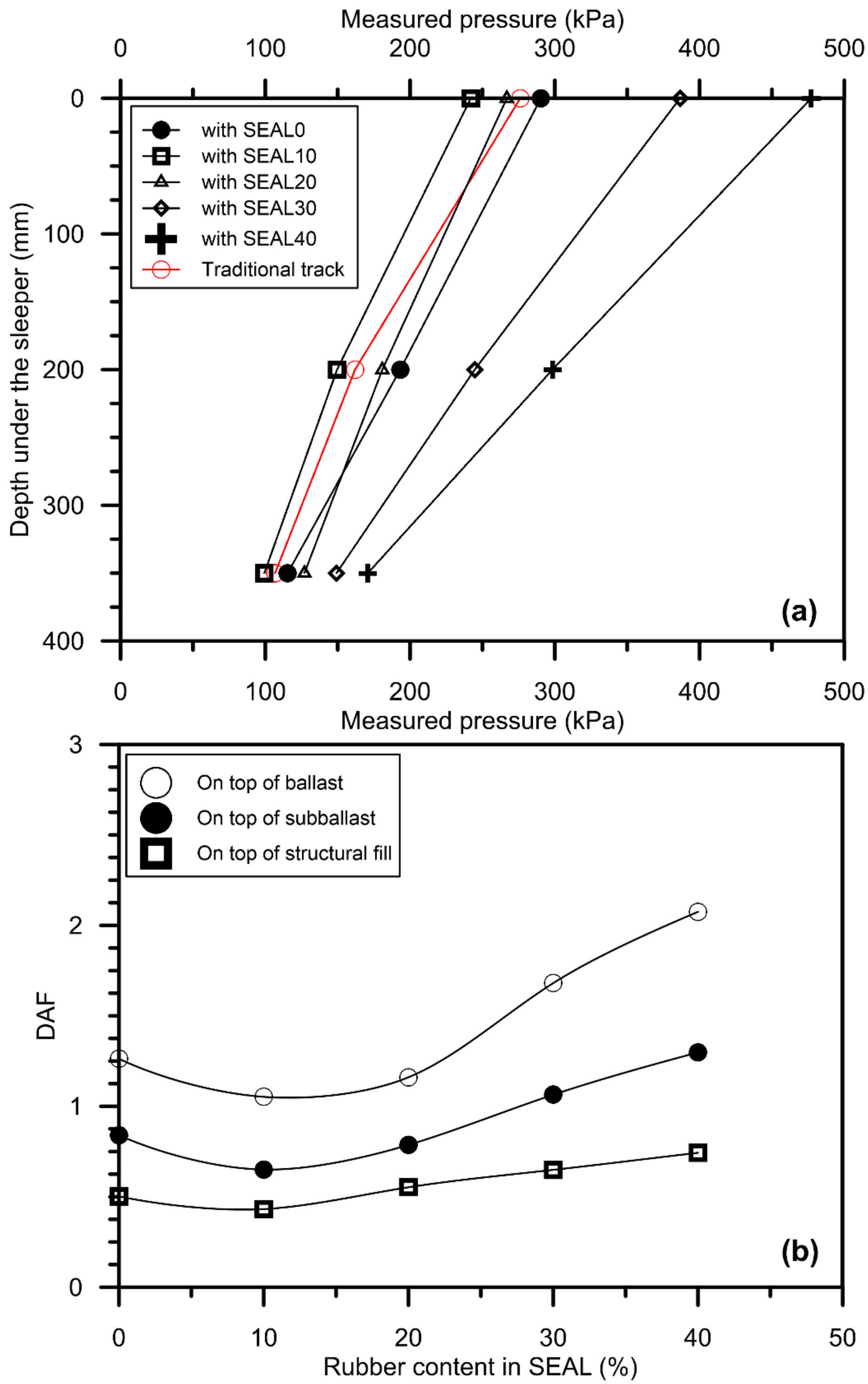

Fig. 10 (a) Measured pressure on top of each layer (i.e. ballast, subballast and structural fill) for each test; (b) DAF for track specimen changing with RC contents within SEAL matrix

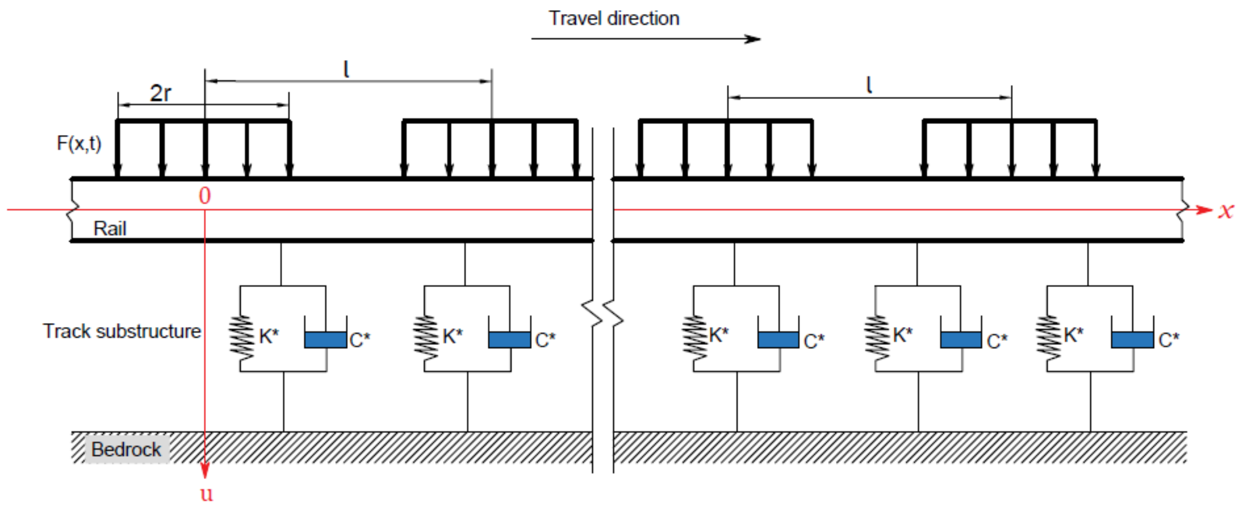

Fig. 11 A rail track subjected to a platoon of uniform moving line loads

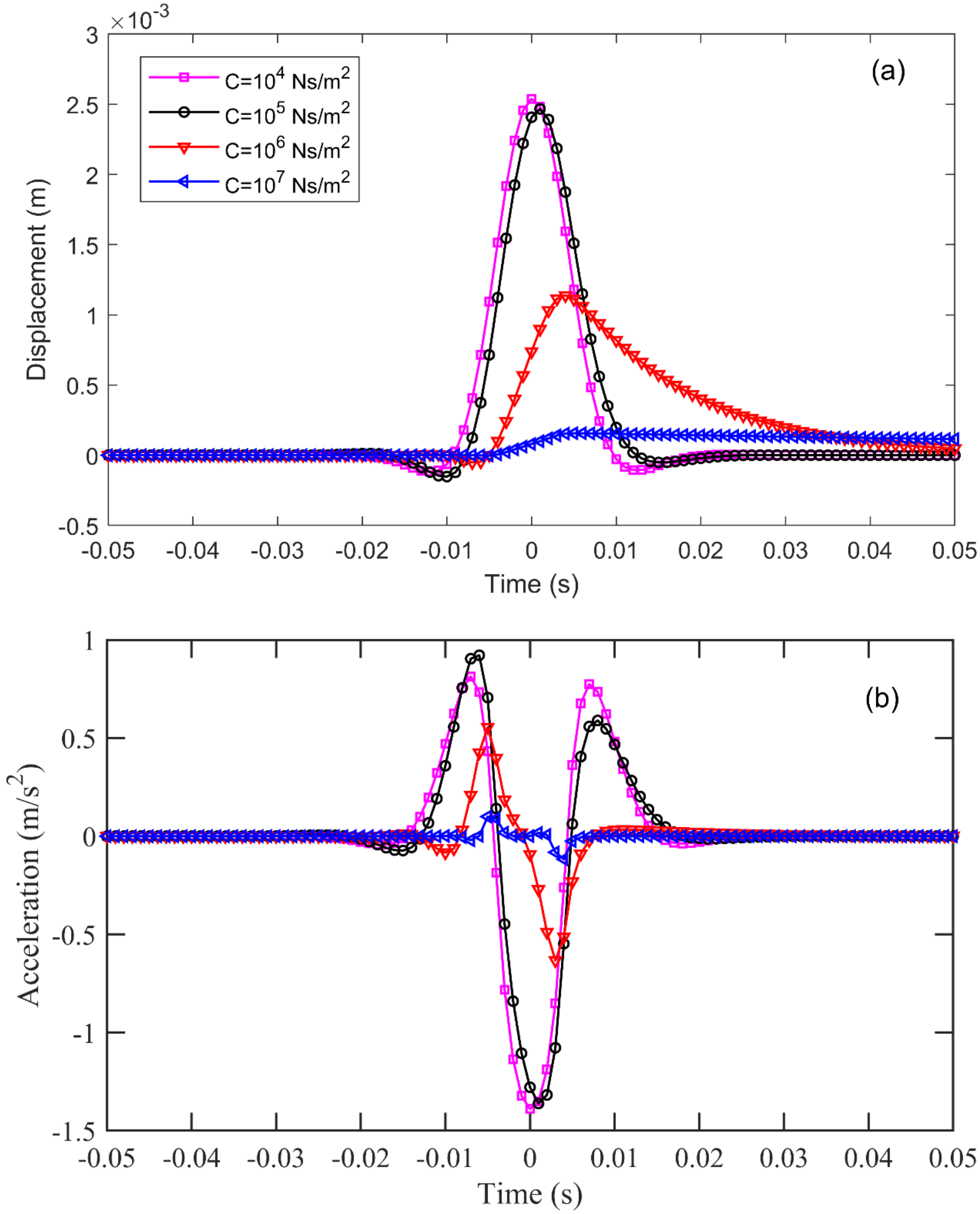

Fig. 12 Dynamic response of rail with changing viscous damping coefficients: (a) displacement and (b) acceleration

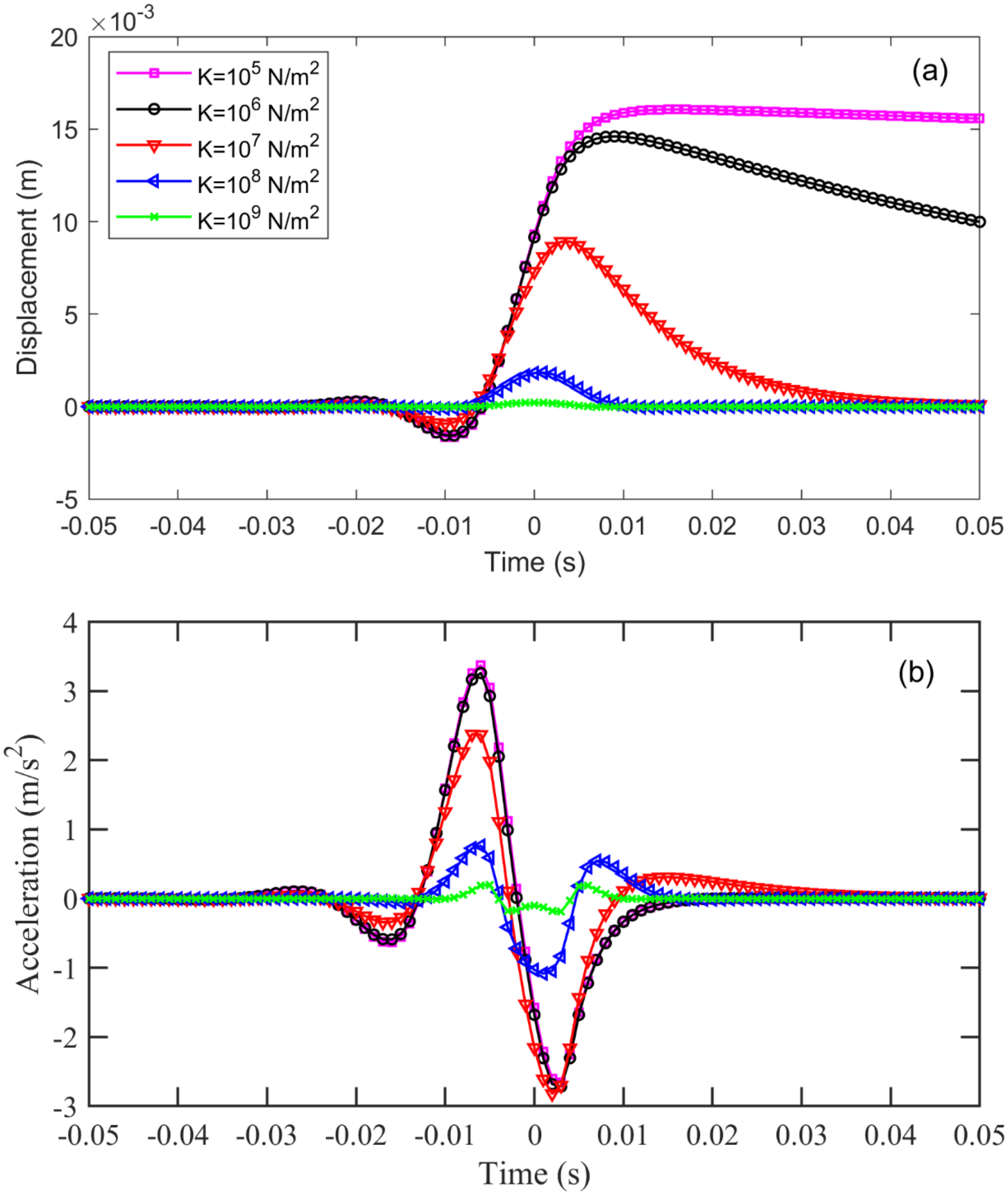

Fig. 13 Dynamic response of rail with changing shear stiffness: (a) displacement and (b) acceleration

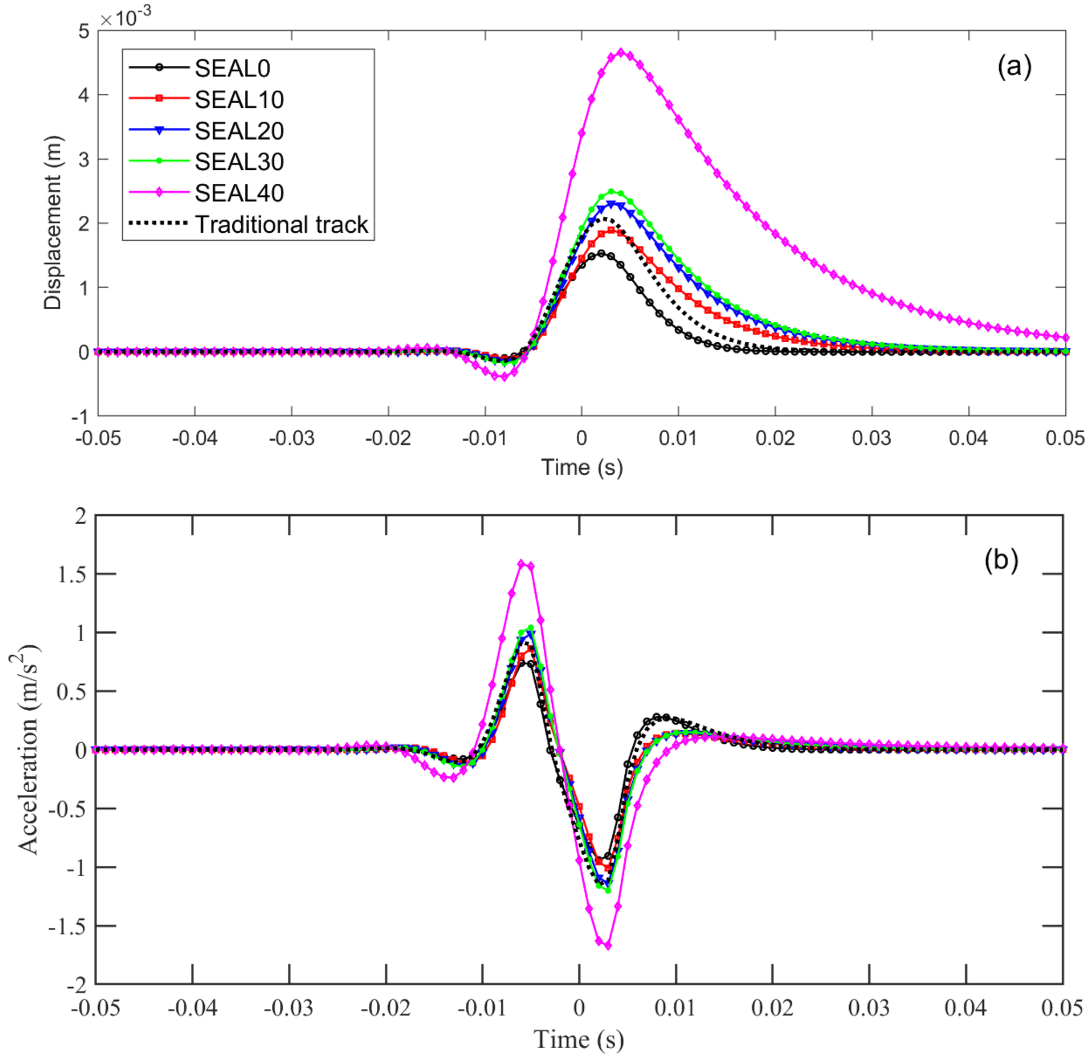

Fig. 14 Predicted rail dynamic response for traditional track and track incorporated with SEAL (a) displacement and (b) acceleration

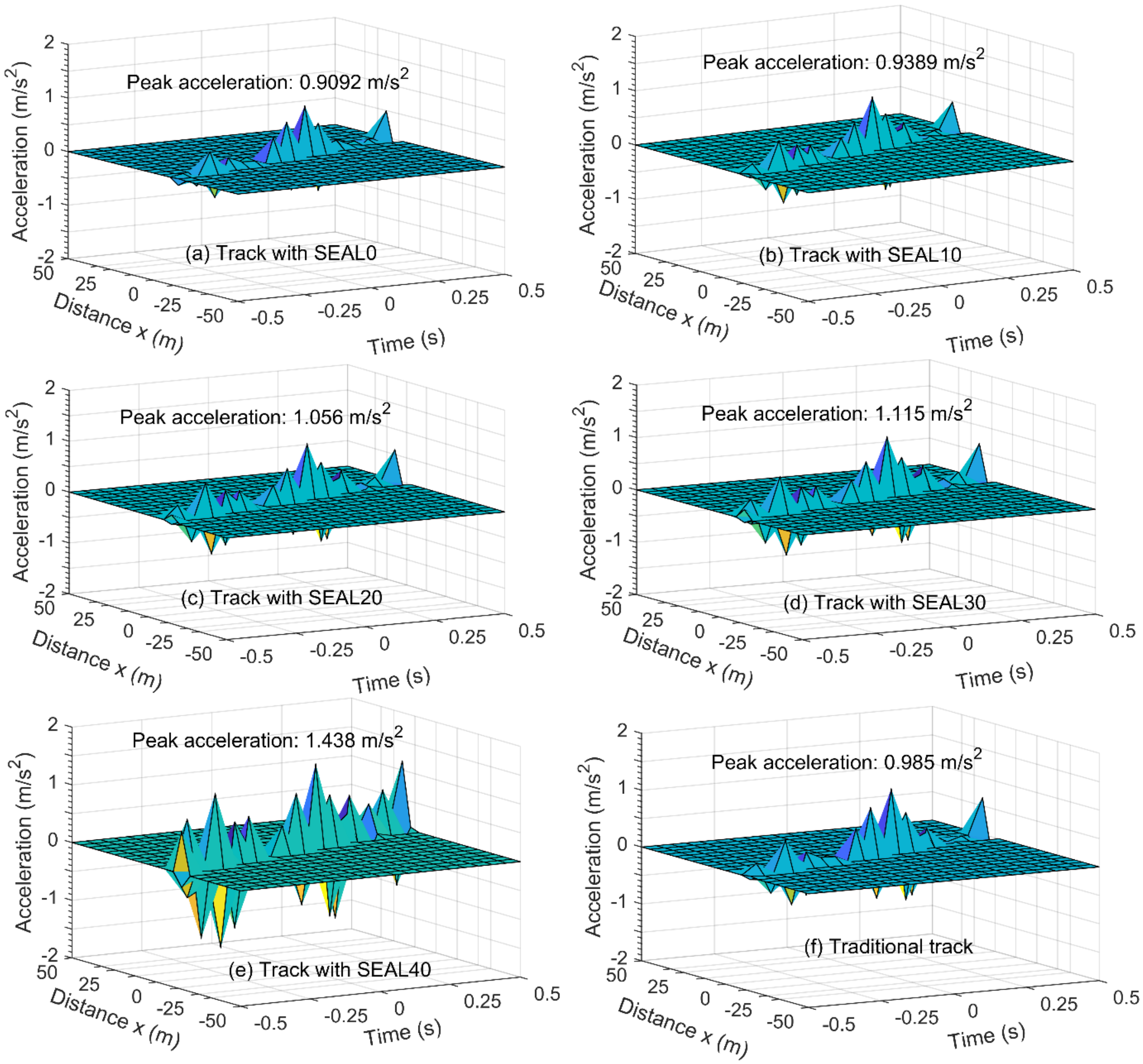

Fig. 15 Predicted 3-D view of the acceleration for the track with (a) SEAL0, (b) SEAL10, (c) SEAL20, (d) SEAL30 and (e) SEAL40 and (f) traditional materials